ARTICLE

Visualizing the Alignment of Lone Pair Electrons in $La_3AsS_5Br_2$ and $La_5As_2S_9Cl_3$ to Form an Acentric or Centrosymmetric Structure

Received 00th January 20xx,
Accepted 00th January 20xx

DOI: 10.1039/x0xx00000x

Andrea Cicirello [a], Andrew Swindle [b], Jian Wang [a, *]

Acentric structures host numerous important applications such as second harmonic generation, nonreciprocal responses, etc. In this work, a heteroanionic system of $La_3AsS_5Br_2$ and $La_5As_2S_9Cl_3$ exhibits a good example of how the alignment of lone pair electrons affects crystal structure. Noncentrosymmetric (NCS) chalcohalide $La_3AsS_5Br_2$, isostructural to $Pr_3AsS_5Cl_2$, and centrosymmetric chalcohalide $La_5As_2S_9Cl_3$ were successfully synthesized by a salt flux growth method. Crystal structures were determined by single crystal X-ray diffraction. Both compounds contain trigonal pyramidal [AsS_3] units with stereochemically active lone pairs in As^{3+}, aligning in the same direction in $La_3AsS_5Br_2$ and in opposite directions in $La_5As_2S_9Cl_3$, which account for their acentric crystal structure and centrosymmetric structure, respectively. Electron localization function (ELF) calculations confirmed that the alignment of the [AsS_3] motifs contributes to the acentric nature of $La_3AsS_5Br_2$. $La_3AsS_5Br_2$ is predicated to be an indirect bandgap semiconductor by theory calculations with a bandgap of 2.27 eV, which is verified by UV-Vis spectrum measurements of 2.8(1) eV. The acentric structural nature of $La_3AsS_5Br_2$ was demonstrated by a moderate second harmonic generation (SHG) response of 0.23×$AgGaS_2$, where $La_5As_2S_9Cl_3$ exhibited no response under the same condition.

Introduction

Compared with centrosymmetric solids, acentric solids draw growing attention from the research community due to the chance of studying directional physical properties such as second harmonic generation [1-15], nonreciprocal responses [16-21], etc. From a chemistry perspective, various strategies have proved efficient to influence the creation of a noncentrosymmetric (NCS) structure, including incorporating second order Jahn-Teller distortion [22-23] and conjugated structure motifs such as distorted FeS_4[14, 24] or GeS_4 tetrahedra [25, 26], WO_5 [27], LaO_6Br_3 [28], etc. Another systematic way to influence a NCS structure is through incorporating atoms with stereochemically active lone pairs (SCALP), including Tl^+, Sn^{2+}, Pb^{2+}, As^{3+}, Sb^{3+}, Bi^{3+}, Te^{4+}, etc., with many successful examples such as Tl^+ in $Tl_4(OH)_2CO_3$[29], $TlXF_3$ (X = Be, Sr)[30]; Sn^{2+} in $Sn_2P_2S_6$[31-33], Sn_2PO_4X (X = F, Cl)[34], $Sn[B_2O_3F_2]$[35]; Pb^{2+} in $Pb_2P_2S_6$[36], $Pb_3P_2S_8$[15], $Pb_{13}O_6Cl_4Br_{10}$[37], $Pb_{13}O_6Cl_7Br_7$[37], and $Pb_{13}O_6Cl_9Br_5$ [37]; As^{3+} in K_3AsS_4[38], Li_3AsS_3[38], $Pb_9As_4S_{15}$[38] and Ag_3AsS_3[38]; Sb^{3+} in $KSbP_2S_6$[39], La_2CuSbS_5[40]; Bi^{3+} in BiB_3O_6[41], $KBiP_2S_6$[39], etc. In addition to affecting crystal structure, SCALP also play a role in enhancing second harmonic generation (SHG) response [42-44]. Hence, the study of how SCALP contributes to the formation of acentric structures is an important topic.

In this work, we report two heteroanionic chalcohalides, $La_3AsS_5Br_2$ and $La_5As_2S_9Cl_3$. $La_3AsS_5Br_2$ and $La_5As_2S_9Cl_3$, which exhibit structural similarity, crystallize in an acentric structure and centrosymmetric structure, respectively. The alignment of SCALP plays an important role in the structural difference, which is confirmed by structure analysis and ELF calculations. This work confirms the importance of the alignment of SCALP in influencing crystal structure. The synthesis, crystal growth, crystal and electronic structures, linear and nonlinear optical properties of two heteroanionic chalcohalides, $La_3AsS_5Br_2$ and $La_5As_2S_9Cl_3$, are summarized in this work.

Experimental Details

Synthesis: All starting materials were stored and used in an Ar-filled glove box. Starting materials were used as received: La powder (Alfa Aesar, 99.7%), As powder (Fisher Scientific, 99%), S powder (Alfa Aesar, 99.5%), $LaBr_3$ (Alfa Aesar, 99.9%), NaBr (Fisher Scientific, 99+%), $LaCl_3$ (Alfa Aesar, 99.9%), NaCl (Sigma-Aldrich, ≥99%). La_2S_3 precursor was produced via stoichiometric ratios of La and S sealed under vacuum in a carbonized silica ampule annealed in a muffle furnace at 773K for 96h, then opened and stored in the glovebox.

$La_3AsS_5Br_2$ Synthesis: A molar ratio of La_2S_3:$LaBr_3$:As:S=7:4:6:9 (total 0.4g) with a mixture of $LaBr_3$:NaBr = 0.66:0.33 (total 0.4g) as a salt flux was placed into a carbonized silica ampule of a diameter of 9mm and flame sealed under high vacuum (<100 mTorr) and placed into a muffle furnace. The ampule was heated to 1123K in 20 hours, annealed at that temperature for 96 hours, and cooled to room temperature in 24 hours. The ampule was opened, and the sample was washed with deionized (DI) water to remove the salt flux, leaving yellow-green mm-sized crystals.

$La_5As_2S_9Cl_3$ Synthesis: A molar ratio of La_2S_3:$LaCl_3$:As:S = 2:1:2:3 (total 0.4g) with a mixture of $LaCl_3$:NaBr = 0.66:0.33 (total 0.4g) as a salt flux was placed into a carbonized silica ampule and sealed under vacuum and heated as the same parameters and temperature profile as $La_3AsS_5Br_2$. The sample was washed with DI water to remove the flux, leaving green mm-sized crystals.

[a] Department of Chemistry and Biochemistry, Wichita State University, Wichita, Kansas 67260, United States
[b] Department of Geology, Wichita State University, Wichita, Kansas 67260, United States

Electronic Supplementary Information (ESI) available: Crystallographic data, photo of crystals, room temperature powder X-ray diffraction data, crystal structure plots. See DOI: 10.1039/x0xx00000x

Single Crystal X-Ray Diffraction (SXRD): Data collections were performed at room temperature for $La_3AsS_5Br_2$ and $La_5As_2S_9Cl_3$ using a Bruker X8 Spectrometer diffractometer equipped with Cu source (λ = 1.5406 Å). Data reduction and integration, together with global unit cell refinements, were performed in the APEX4 software.[45] Multi-scan absorption corrections were applied.[45] The structures were solved by direct methods and refined by full matrix least-squares methods on F^2 using the SHELX package with anisotropic displacement parameters for all atoms.[46] Details of the data collection and structure refinement are provided in **Table 1**. Atomic coordinates and selected distances are listed in **Tables S1 and S2**. Crystallographic data for $La_3AsS_5Br_2$ and $La_5As_2S_9Cl_3$ have been deposited to the Cambridge Crystallographic Data Centre, CCDC, 12 Union Road, Cambridge CB21EZ, UK. Copies of the data can be obtained free of charge by quoting the depository numbers CCDC- 2281773 ($La_3AsS_5Br_2$) and CCDC- 2281774 ($La_5As_2S_9Cl_3$).

Table 1. Selected crystal data and unit cell parameters for $La_3AsS_5Br_2$ and $La_5As_2S_9Cl_3$

Empirical Formula	$La_3AsS_5Br_2$	$La_5As_2S_9Cl_3$
Formula weight	811.77	1239.28
Temperature	296(2) K	
Radiation, wavelength	Cu-Kα, 1.54718 Å	
Crystal system	Monoclinic	Orthorombic
Space group	*Cc* (No. 9)	*Pbcm* (No. 57)
Unit cell dimensions	a = 22.3092(14) Å b = 7.1387(5) Å c = 7.1638 (5) Å β = 98.471(2)	a = 7.0472(3) Å b = 7.1152(3) Å c = 37.1137 (13) Å
Unit cell volume	1128.45(13) Å^3	1860.96 (13) Å^3
Z	4	4
Density (calc)	4.778 cm^3	4.423 g/cm^3
Absorption coefficient	105.859 mm^{-1}	103.931 mm^{-1}
Final R indices [I > 2σ(I)]	R_1=0.0444; wR_2=0.1058	R_1=0.0398; wR_2=0.1123
Final R indices [all data]	R_1=0.0444; wR_2=0.1058	R_1=0.0414; wR_2=0.1138

Powder X-Ray Diffraction (PXRD): Data were collected at room temperature using a Rigaku MiniFlex 6G diffractometer with Cu-*K*α radiation (λ =1.5406 Å).

UV-Vis Measurements: Diffuse-reflectance spectra of $La_3AsS_5Br_2$ and $La_5As_2S_9Cl_3$ powder samples were recorded at room temperature by a PERSEE-T8DCS UV-Vis spectrophotometer equipped with an integration sphere in the wavelength range of 230−850 nm. The reflectance data, R, were recorded and converted to the Kubelka-Munk function, $f(R)=(1-R)^2(2R)^{-1}$. Tauc plots,[47-48] $(KM*E)^2$ and $(KM*E)^{1/2}$, were applied to estimate direct and indirect band gap, respectively.

TB-LMTO-ASA simulations: Electronic structures, including band structures and density of states (DOS), of $La_3AsS_5Br_2$ were calculated using the tight binding-linear muffin tin orbitals-atomic sphere approximation (TB-LMTO-ASA) program. [49-50] The von-Barth-Hedin exchange potential was employed for the LDA calculations.[49] The radial scalar-relativistic Dirac equation was solved to obtain the partial waves. The density of states and band structures were calculated after converging the total energy on a dense k-mesh of $La_3AsS_5Br_2$ (16×16×8 points with 1088 irreducible k-points).

Second Harmonic Measurements: Using the Kurtz and Perry method,[51] powder SHG responses of $La_3AsS_5Br_2$ were investigated by a Q-switch laser (2.09 μm, 3 Hz, 50 ns) with various particle sizes, including 38.5–54, 54–88, 88–105, 105–150, and 150–200 μm. Homemade $AgGaS_2$ was selected as the reference. The lab-synthesized $AgGaS_2$ crystals were ground to the same size range as $La_3AsS_5Br_2$ compound.

Results and Discussion

Synthesis and Crystal Growth

Mm-sized crystals of $La_3AsS_5Br_2$ and $La_5As_2S_9Cl_3$ were successfully grown via a salt-flux method (**Figure S1**). The mm-sized crystals were collected after washing with DI water to remove the salt flux. **Figures S2** and **S3** shows a comparison of theoretical and experimental PXRD patterns for $La_3AsS_5Br_2$ (a) and $La_5As_2S_9Cl_3$ (b), which verified the single-phase nature of $La_3AsS_5Br_2$ and $La_5As_2S_9Cl_3$

Crystal Structure

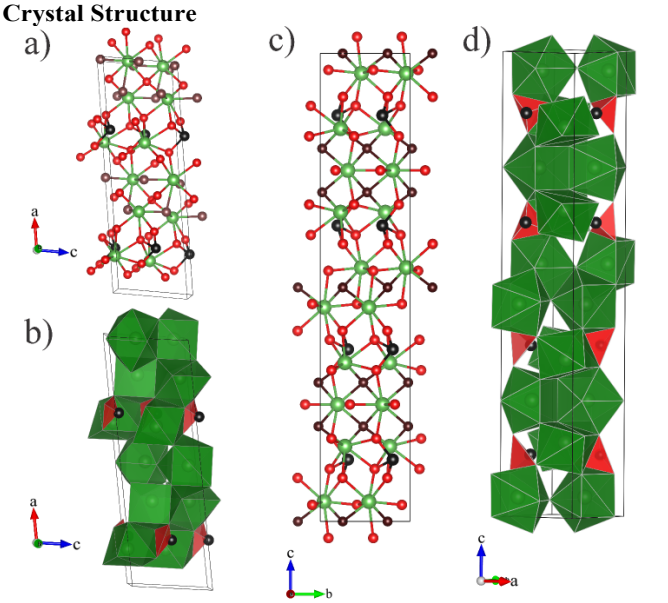

Figure 1. Ball and stick models of $La_3AsS_5Br_2$ (a) and $La_5As_2S_9Cl_3$ (c). Polyhedral models of $La_3AsS_5Br_2$ (b) and $La_5As_2S_9Cl_3$ (d). La: green, As: black, S: red, Br: light brown, Cl : dark brown.

$La_3AsS_5Br_2$: $La_3AsS_5Br_2$ crystallizes in the acentric monoclinic space group *Cc* (No. 9), which belongs to the known $La_3AsS_5Cl_2$ structure type.[52] Other isostructural compounds of $Pr_3AsS_5Cl_2$ [53], $La_3SbS_5Cl_2$[54] and $Ce_3SbS_5Cl_2$,[55] were also reported. Selected crystal data and parameters are listed in **Tables 1, S1 and S2**. The crystal structure of $La_3AsS_5Br_2$ is presented in **Figures 1a** and **1b**. There are three unique La atoms at Wyckoff site *4a*, one unique As atom at Wyckoff site *4a*, five unique S atoms at Wyckoff site *4a*, and two unique Br atoms at Wyckoff site *4a*. All atoms occupy their sites with full occupancy. The three-dimensional framework of $La_3AsS_5Br_2$ is constructed by [$La1S_5Br_3$] bicapped trigonal prisms, [$La2S_5Br_3$] bicapped trigonal prisms, [$La3S_7$] capped trigonal prisms, and [$As1S_3$] trigonal pyramids, which are interlinked to each other. The polyhedral structure model of $La_3AsS_5Br_2$ is shown in **Figure 1b**. The constructing units of $La_3AsS_5Br_2$ is shown in **Figure S4**. During our efforts to synthesize a Cl analogue of $La_3AsS_5Br_2$, a centrosymmetric $La_5As_2S_9Cl_3$ was found as the product. $La_5As_2S_9Cl_3$ crystallizes in the centrosymmetric orthorhombic space group *Pbcm* (No. 57), which belongs to the known $La_5Sb_2S_9Cl_3$[55] structure type. Selected crystal data and parameters are listed in **Tables 1, S1 and S2**. There are three unique La atoms: La1 at Wyckoff site *4d* and La2 and La3 at Wyckoff site *8e*, one unique As atom at Wyckoff site *8e*, five unique S atoms: S1, S2, S3, and S4 at Wyckoff site *8e* and S5 at Wyckoff site *4d*, and two unique Cl atoms, Cl1 at Wyckoff site *4c* and Cl2 at Wyckoff site *8e*. All atoms occupy their sites with

full occupancy. The three-dimensional framework of $La_5As_2S_9Cl_3$ is constructed by [La1S_4Cl_4] bicapped trigonal prisms, [La2S_5Cl_2] capped trigonal prisms, [La3S_6Cl_2] bicapped trigonal prisms and [As1S_3] trigonal pyramids, which are interlinked to each other. The polyhedral structure model and constructing units of $La_5Sb_2S_9Cl_3$ is shown in **Figure 1d** and **Figure S5**, respectively.

The La-S interactions within $La_3AsS_5Br_2$ fall into the range of 2.87(1)-3.15 (1) Å, which are comparable to the La-S interactions within $La_5As_2S_9Cl_3$ of 2.81(7)-3.14 (4) Å and many lanthanum-sulfide compounds such as $La_4Ge_3S_{12}$ (2.864-3.245 Å) [25], $La_6Pd_{0.96}Si_2S_{14}$ (2.817-3.164 Å) [56], $La_5Sb_2S_9Cl_3$(2.841-3.106 Å) [55], $La_3SbS_5Cl_2$ (2.833-3.117 Å) [55], La_3LiSnS_7 (2.848-3.297 Å) [57], etc. The La-Br interactions within $La_3AsS_5Br_2$ of 3.04 (3)-3.44(3) Å are longer than La-Cl interactions within $La_5As_2S_9Cl_3$ of 2.83(1)-2.97(1) Å, which is expected due to the larger ionic size of Br^- than Cl^-. The As-S interactions are 2.26(1)-2.27(1) Å and 2.25(5)-2.28(5) Å for $La_5As_2S_9Cl_3$ and $La_3AsS_5Br_2$, respectively, which are close to many arsenic-sulfide compounds such as As_4S_4 (2.21-2.27Å) [58], $Ba_2(As_{1.5}Bi_{0.5})S_5$ (2.21-2.43Å) [59], $CsCu_2AsS_3$(2.24-2.27 Å) [60], $Cs_2Ag_2As_2S_5$ (2.24-2.31 Å) [61], KCu_2AsS_3 (2.26-2.30 Å) [62], etc. In addition to comparable interatomic distances, each unit cell of $La_5As_2S_9Cl_3$ and $La_3AsS_5Br_2$ is constructed by the same polyhedra: two [LaX8] bicapped trigonal prisms, one [LaX7] capped trigonal prism, and one [AsS_3] trigonal pyramid, where the X represents various combinations of S atoms and Cl atoms or Br atoms (**Figures S3** and **S4**). There are two axes of $La_5As_2S_9Cl_3$ with similar length to $La_5As_2S_9Cl_3$ (**Table 1**). The structural similarity between $La_5As_2S_9Cl_3$ and $La_3AsS_5Br_2$ is obvious. What is the chemical reason for the structural difference between $La_5As_2S_9Cl_3$ and $La_3AsS_5Br_2$? Understanding how to form acentric structures is very important for studying directional physical properties [1-21].

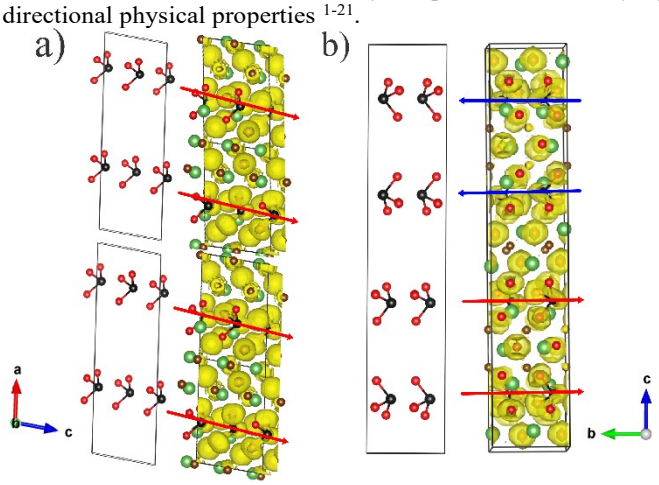

Figure 2. ELF of $La_3AsS_5Br_2$ (a) and $La_5As_2S_9Cl_3$ (b) emphasizing the alignment of SCALP of AsS_3 motifs with η=0.65. The alignment of AsS_3 motifs is shown on the left of ELF figure with removal of La, Br, and Cl atoms. The arrows are added artificially to emphasize the alignment of SCALP of AsS_3 motifs. To compare the structure of $La_3AsS_5Br_2$ and $La_5As_2S_9Cl_3$, two unit cells of $La_3AsS_5Br_2$ are presented. La: green, Br/Cl: brown, As: black, S: red.

As shown in **Figures 1** and **2**, one hypothesis would be the alignment of SCALP in [AsS_3] motifs plays an important role in driving the crystal structure from acentric $La_3AsS_5Br_2$ to centrosymmetric $La_5As_2S_9Cl_3$. To better understand the role of the alignment of [AsS_3] motifs in both structures, the ELF simulations were employed, which are shown in **Figure 2**. The ELF of $La_3AsS_5Br_2$ and $La_5As_2S_9Cl_3$ are shown in **Figures 2a** and **2b**, respectively. **Figure 2a** shows the alignment of SCALP of [AsS_3] motifs in the same direction in the structure of $La_3AsS_5Br_2$, producing a directional dipole moment which contributes to its acentric structure. **Figure 2b** shows the alignment of SCALP of [AsS_3] motifs in opposing directions in $La_5As_2S_9Cl_3$, resulting in a cancelled dipole moment, contributing to its centrosymmetric structure. Please also note, the reason for forming acentric structures is complex, the connectivity of polyhedra within $La_3AsS_5Br_2$ and $La_5As_2S_9Cl_3$ is also distinct, which also contributes to the structural difference. Second harmonic generation measurements were employed to confirm the acentric nature and centrosymmetric nature of $La_3AsS_5Br_2$ and $La_5As_2S_9Cl_3$, respectively.

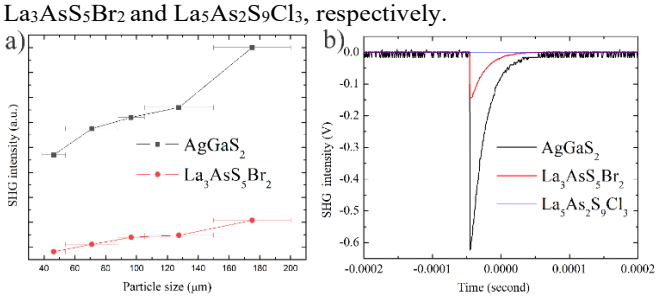

Figure 3. (a) Second harmonic generation response of $La_3AsS_5Br_2$ compared to $AgGaS_2$ (AGS) in varying particle size ranges. (b) SHG measurement of $La_3AsS_5Br_2$ and $La_5As_2S_9Cl_3$ with AGS measured at the same conditions as a reference.

SHG measurements were taken for $La_3AsS_5Br_2$ and $La_5As_2S_9Cl_3$ in varying particle sizes and compared to AGS (**Figure 3a**), which confirmed the acentric nature of $La_3AsS_5Br_2$. $La_3AsS_5Br_2$ is a Type-I phase matchable compound, in which the SHG intensity increases with increasing particle size. The SHG response of $La_3AsS_5Br_2$ is about 0.23× AGS for the sample of 150-200 μm particle size. There was no signal of SHG response detected from $La_5As_2S_9Cl_3$ (**Figure 3b**), which indicates its centrosymmetric nature and agrees well with single crystal X-ray diffraction refinement results. Even though the SHG response of $La_3AsS_5Br_2$ is not very high, the easily grown nature, excellent air stability, and moderate bandgap (*vide infra*) still make $La_3AsS_5Br_2$ attractive for infrared nonlinear application. To further study the properties of $La_3AsS_5Br_2$, electronic structures were calculated and shown in **Figure 4**.

Band Structure Calculations

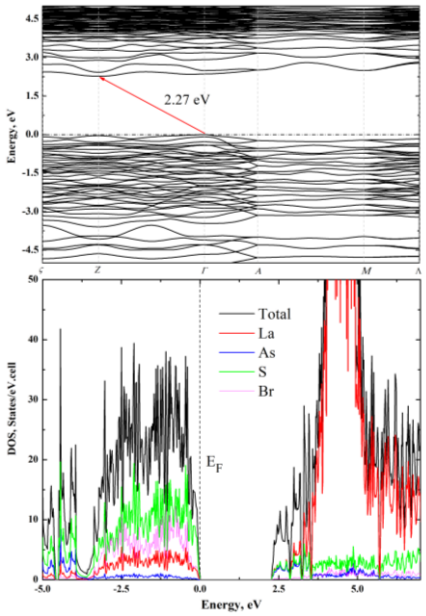

Figure 4. Theoretical band structure (top) and density of states (DOS) (bottom) of $La_3AsS_5Br_2$.

The band structure of $La_3AsS_5Br_2$ is presented in **Figure 4** top. The top of the valence band is found at the *Γ* points and the bottom of the conduction band is located at the *Z* points. This predicts $La_3AsS_5Br_2$ as an indirect band gap semiconductor with a theoretical band gap of 2.27 eV. The semiconductor nature of $La_3AsS_5Br_2$ is also supported by the charge-balanced formula $(La^{3+})_3(As^{3+})(S^{2-})_5(Br^-)_2$ by assigning a formal charge of 3+ to the La atoms, 3+ to the As atoms, 2- to the S atoms, and 1- to the Br atoms. The trivalent nature of the As atoms are confirmed with the presence of SCALP (**Figure 2**). The charge balanced formula $(La^{3+})_5(As^{3+})_2(S^{2-})_9(Cl^-)_3$ of $La_5As_2S_9Cl_3$ can be established by the same way as $La_3AsS_5Br_2$. As shown in the DOS in **Figure 4** bottom and Figure S6, the top of the valence band is mainly contributed by S 2p orbitals and Br 2p orbitals, with some contributions by La orbitals. The bottom of the conduction band is composed of As 3p orbitals, S 2p orbitals, and La orbitals. The optical properties of $La_3AsS_5Br_2$ are predominantly contributed by As-S interactions and La-S interactions, with some contributions from La-Br interactions. To improve the SHG response, bandgap engineering such as replacing As by Sb or S by Se would be an applicable way [25]. The semiconducting nature of $La_3AsS_5Br_2$ was verified by UV-Vis spectrum measurements.

Linear Optical Properties

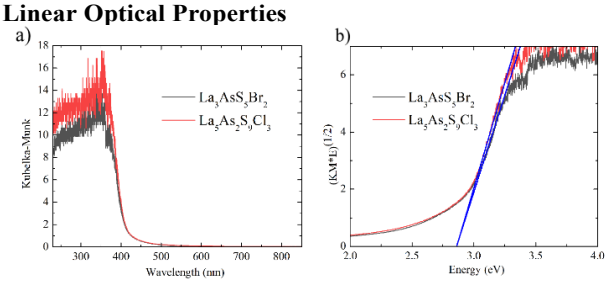

Figure 5. (a) Kubelka-Munk of $La_3AsS_5Br_2$ and $La_5As_2S_9Cl_3$. (b) Indirect Tauc plots of $La_3AsS_5Br_2$ and $La_5As_2S_9Cl_3$.

The optical bandgaps of $La_3AsS_5Br_2$ and $La_5As_2S_9Cl_3$ were determined via solid-state UV-Vis diffuse reflectance spectroscopy (**Figure 5**). $La_3AsS_5Br_2$ and $La_5As_2S_9Cl_3$ both possess strong absorption edges around 400-475 nm, which agrees well with their green color appearance. $La_3AsS_5Br_2$ was determined to be an indirect bandgap semiconductor via theoretical calculations (**Figure 4**). The indirect allowed transition of $La_3AsS_5Br_2$ was determined to be 2.83(5) eV for $La_3AsS_5Br_2$, which is close to the theoretically predicted value of 2.27 eV. The indirect allowed transition of $La_5As_2S_9Cl$ was determined to be 2.87(5) eV. For infrared nonlinear optical applications, large laser damage threshold (LDT) is also required, which is proportional to bandgap. The incorporation of electronegative anions into compounds is shown to result in a large band gap [39]. The moderate band gap of $La_3AsS_5Br_2$ might result in high LDT for $La_3AsS_5Br_2$, which is undergoing analysis now.

Conclusion

Two arsenic-containing lanthanum chalcohalides have been synthesized for the first time: $La_3AsS_5Br_2$ and $La_5As_2S_9Cl_3$. Both compounds contain trigonal pyramidal $[AsS_3]$ motifs, with the centrosymmetric $La_5As_2S_9Cl_3$ aligning the motifs in opposite directions and the noncentrosymmetric $La_3AsS_5Br_2$ aligning the motifs in the same direction. The alignment of the motifs contributes to the shifting of the structure from centrosymmetric in the chloride to noncentrosymmetric in the bromide. $La_5As_2S_9Cl_3$ is shown to have an indirect bandgap of 2.87(5) eV. $La_3AsS_5Br_2$ is shown to have an indirect bandgap of 2.83(5) eV, and a moderate SHG response of 0.23×AGS. These heteroanionic compounds exhibit a good example to study how the alignment of SCALP of $[AsS_3]$ motifs affects crystal structure. Moderate SHG response, easy growth of large crystals, excellent ambient stability, and moderate bandgap of $La_3AsS_5Br_2$ indicates its potential application as an infrared nonlinear optical material.

Author Contributions

A. Cicirello: Validation, Visualization, Investigation, Methodology, Writing – original draft; A. Swindle: Resource, Writing – review & editing. J. Wang: Investigation, Methodology, Funding acquisition, Supervision, Writing – original draft, Writing – review & editing,

Conflicts of interest

There are no conflicts to declare.

Acknowledgements

This research was supported by National Science Foundation (DMR-2316811). J. Wang would like to thank Prof. Bingbing Zhang from Hebei University for measuring second harmonic generation response of $La_3AsS_5Br_2$.

Notes and references

[1] M. Yu, Y. Okawachi, A. G. Griffith, N. Picqué, M. Lipson and A. L. Gaeta, Silicon-chip-based mid-infrared dual-comb spectroscopy, *Nat Commun*, 2018, **9**, 1869.

[2] V. Muraviev, V. O. Smolski, Z. E. Loparo and K. L. Vodopyanov, Massively parallel sensing of trace molecules and their isotopologues with broadband subharmonic mid-infrared frequency combs, *Nature Photon*, 2018, **12**, 209–214.

[3] J. S. Dam, P. Tidemand-Lichtenberg and C. Pedersen, Room-temperature mid-infrared single-photon spectral imaging, *Nature Photon*, 2012, **6**, 788–793.

[4] D. Pestov, X. Wang, G. O. Ariunbold, R. K. Murawski, V. A. Sautenkov, A. Dogariu, A. V. Sokolov and M. O. Scully, Single-shot detection of bacterial endospores via coherent Raman spectroscopy, *Proc. Natl. Acad. Sci. U.S.A.*, 2008, **105**, 422–427.

[5] K. M. Ok, Toward the Rational Design of Novel Noncentrosymmetric Materials: Factors Influencing the Framework Structures, *Acc. Chem. Res.*, 2016, **49**, 2774–2785.

[6] Chung and M. G. Kanatzidis, Metal Chalcogenides: A Rich Source of Nonlinear Optical Materials, *Chem. Mater.*, 2014, **26**, 849–869.

[7] L. Kang, M. Zhou, J. Yao, Z. Lin, Y. Wu and C. Chen, Metal Thiophosphates with Good Mid-infrared Nonlinear Optical Performances: A First-Principles Prediction and Analysis, *J. Am. Chem. Soc.*, 2015, **137**, 13049–13059.

[8] D. Mei, W. Cao, N. Wang, X. Jiang, J. Zhao, W. Wang, J. Dang, S. Zhang, Y. Wu, P. Rao and Z. Lin, Breaking through the "3.0 eV wall" of energy band gap in mid-infrared nonlinear optical rare earth chalcogenides by

charge-transfer engineering, *Mater. Horiz.*, 2021, **8**, 2330–2334.

[9] F. Liang, L. Kang, Z. Lin and Y. Wu, Mid-Infrared Nonlinear Optical Materials Based on Metal Chalcogenides: Structure–Property Relationship, *Cryst. Growth Des.*, 2017, **17**, 2254–2289.

[10] X. Cui, J. Xiao, Y. Wu, P. Du, R. Si, H. Yang, H. Tian, J. Li, W.-H. Zhang, D. Deng and X. Bao, A Graphene Composite Material with Single Cobalt Active Sites: A Highly Efficient Counter Electrode for Dye-Sensitized Solar Cells, *Angew. Chem. Int. Ed.*, 2016, **55**, 6708–6712.

[11] Wu, B. Zhang, Z. Yang and S. Pan, New Compressed Chalcopyrite-like $Li_2BaM^{IV}Q_4$ (M^{IV} = Ge, Sn; Q = S, Se): Promising Infrared Nonlinear Optical Materials, *J. Am. Chem. Soc.*, 2017, **139**, 14885–14888.

[12] H.-Y. Chang, S.-H. Kim, P. S. Halasyamani and K. M. Ok, Alignment of Lone Pairs in a New Polar Material: Synthesis, Characterization, and Functional Properties of $Li_2Ti(IO_3)_6$, *J. Am. Chem. Soc.*, 2009, **131**, 2426–2427.

[13] H. Zhang, M. Zhang, S. Pan, X. Dong, Z. Yang, X. Hou, Z. Wang, K. B. Chang and K. R. Poeppelmeier, $Pb_{17}O_8Cl_{18}$: A Promising IR Nonlinear Optical Material with Large Laser Damage Threshold Synthesized in an Open System, *J. Am. Chem. Soc.*, 2015, **137**, 8360–8363.

[14] B. Ji, K. Pandey, C. P. Harmer, F. Wang, K. Wu, J. Hu and J. Wang, Centrosymmetric or Noncentrosymmetric? Transition Metals Talking in $K_2TGe_3S_8$ (T = Co, Fe), *Inorg. Chem.*, 2021, **60**, 10603–10613.

[15] B. Ji, E. Guderjahn, K. Wu, T. H. Syed, W. Wei, B. Zhang and J. Wang, Revisiting thiophosphate $Pb_3P_2S_8$: a multifunctional material combining a nonlinear optical response and photocurrent response, *Phys. Chem. Chem. Phys.*, 2021, **23**, 23696–23702.

[16] Y. Tokura and N. Nagaosa, Nonreciprocal responses from non-centrosymmetric quantum materials, *Nat Commun*, 2018, **9**, 3740.

[17] H. Narita, J. Ishizuka, R. Kawarazaki, D. Kan, Y. Shiota, T. Moriyama, Y. Shimakawa, A. V. Ognev, A. S. Samardak, Y. Yanase and T. Ono, Field-free superconducting diode effect in noncentrosymmetric superconductor/ferromagnet multilayers, *Nat. Nanotechnol.*, 2022, **17**, 823–828.

[18] H. Gao, J. Strockoz, M. Frakulla, J. W. F. Venderbos and H. Weng, Noncentrosymmetric topological Dirac semimetals in three dimensions, *Phys. Rev. B*, 2021, **103**, 205151.

[19] S. Yip, Noncentrosymmetric Superconductors, *Annu. Rev. Condens. Matter Phys.*, 2014, **5**, 15–33.

[20] R. Wakatsuki, Y. Saito, S. Hoshino, Y. M. Itahashi, T. Ideue, M. Ezawa, Y. Iwasa and N. Nagaosa, Nonreciprocal charge transport in noncentrosymmetric superconductors, *Sci. Adv.*, 2017, **3**, e1602390.

[21] M. Li, M. Xia and H. Xiao, Centrosymmetric Versus Noncentrosymmetric: Structural and Optical Studies on Inorganic-Organic Hybrid Compounds of Bismuth Thiourea Iodide Resulting from Acid Effect, *ChemistrySelect*, 2017, **2**, 5882–5886.

[22] Kang, F. Liang, X. Jiang, Z. Lin and C. Chen, First-Principles Design and Simulations Promote the Development of Nonlinear Optical Crystals, *Acc. Chem. Res.*, 2020, **53**, 209–217.

[23] W. Zhang, H. Yu, H. Wu and P. S. Halasyamani, Phase-Matching in Nonlinear Optical Compounds: A Materials Perspective, *Chem. Mater.*, 2017, **29**, 2655–2668.

[24] B. Ji, F. Wang, K. Wu, B. Zhang and J. Wang, d^6 *versus* d^{10} , Which Is Better for Second Harmonic Generation Susceptibility? A Case Study of $K_2TGe_3Ch_8$ (T = Fe, Cd; Ch = S, Se), *Inorg. Chem.*, 2023, **62**, 574–582.

[25] G. Cicirello, K. Wu, B. B. Zhang and J. Wang, Applying band gap engineering to tune the linear optical and nonlinear optical properties of noncentrosymmetric chalcogenides $La_4Ge_3Se_xS_{12-x}$ (x = 0, 2, 4, 6, 8, 10), *Inorg. Chem. Front.*, 2021, **8**, 4914–4923.

[26] G. Cicirello, K. Wu and J. Wang, Synthesis, crystal structure, linear and nonlinear optical properties of quaternary sulfides $Ba_6(Cu_2X)Ge_4S_{16}$ (X=Mg, Mn, Cd), *J. Solid State Chem.*, 2021, **300**, 122226.

[27] T. Schleid and I. Hartenbach, On halide derivatives of rare-earth metal(III) oxidomolybdates(VI) and -tungstates(VI), *Z. Kristallogr. Cryst. Mater.*, 2016, **231**, 449–466.

[28] Z. Jiao, O. M. Mireles, K. Ensz, F. Wang, M. Liang, P. S. Halasyamani, B. Zhang, D. P. Rillema and J. Wang, Heteroanionic $LaBrVIO_4$ (VI=Mo, W): Excellence in Both Nonlinear Optical Properties and Photoluminescent Properties., *Chem. Mater. Accepted.*

[29] O. I. Siidra, S. N. Britvin and S. V. Krivovichev, Hydroxocentered $[(OH)Tl_3]^{2+}$ triangle as a building unit in thallium compounds: synthesis and crystal structure of $Tl_4(OH)_2CO_3$, *Z. Kristallogr.*, 2009, **224**, 563–567.

[30] G. Ayub, A. Rauf, M. Husain, A. Algahtani, V. Tirth, T. Al-Mughanam, A. H. Alghtani, N. Sfina, N. Rahman, M. Sohail, R. Khan, A. Azzouz-Rached, A. Khan, N. H. Al-Shaalan, S. Alharthi, S. A. Alharthy and M. A. Amin, Investigating the Physical Properties of Thallium-Based Ternary $TlXF_3$ (X = Be, Sr) Fluoroperovskite Compounds for Prospective Applications, *ACS Omega*, 2023, **8**, 17779–17787.

[31] Anema, A. Grabar and Th. Rasing, The nonlinear optical properties of $Sn_2P_2S_6$, *Ferroelectrics*, 1996, **183**, 181–183.

[32] J. He, S. H. Lee, F. Naccarato, G. Brunin, R. Zu, Y. Wang, L. Miao, H. Wang, N. Alem, G. Hautier, G.-M. Rignanese, Z. Mao and V. Gopalan, SnP_2S_6: A Promising Infrared Nonlinear Optical Crystal with Strong Nonresonant Second Harmonic Generation and Phase-Matchability, *ACS Photonics*, 2022, **9**, 1724–1732

[33] Z.-H. Shi, M. Yang, W.-D. Yao, W. Liu and S.-P. Guo, $SnPQ_3$ (Q = S, Se, S/Se): A Series of Lone-Pair Cationic Chalcogenophosphates Exhibiting Balanced NLO Activity Originating from SnQ_8 Units, *Inorg. Chem.*, 2021, **60**, 14390–14398.

[34] T. Zheng, Q. Wang, J. Ren, L. Cao, L. Huang, D. Gao, J. Bi and G. Zou, Halogen regulation triggers structural transformation from centrosymmetric to noncentrosymmetric switches in tin phosphate halides Sn_2PO_4X (X = F, Cl), *Inorg. Chem. Front.*, 2022, **9**, 4705–4713.

[35] S. G. Jantz, M. Dialer, L. Bayarjargal, B. Winkler, L. Van Wüllen, F. Pielnhofer, J. Brgoch, R. Weihrich and H. A. Höppe, $Sn[B_2O_3F_2]$-The First Tin Fluorooxoborate as Possible NLO Material, *Adv. Opt. Mater.*, 2018, **6**, 1800497.

[36] B. Ji, A. Sarkar, K. Wu, A. Swindle and J. Wang, $A_2P_2S_6$ (A = Ba and Pb): a good platform to study the polymorph effect and lone pair effect to form an acentric structure, *Dalton Trans.*, 2022, **51**, 4522–4531.

[37] X. Chen, H. Jo and K. M. Ok, Lead Mixed Oxyhalides Satisfying All Fundamental Requirements for High-Performance Mid-Infrared Nonlinear Optical Materials, *Angew. Chem.*, 2020, **132**, 7584–7590.

[38] R. Yin, C. Hu, B.-H. Lei, S. Pan and Z. Yang, Lone pair effects on ternary infrared nonlinear optical materials, *Phys. Chem. Chem. Phys.*, 2019, **21**, 5142–5147.

[39] V. Nguyen, B. Ji, K. Wu, B. Zhang and J. Wang, Unprecedented mid-infrared nonlinear optical materials

achieved by crystal structure engineering, a case study of $(KX)P_2S_6$ (X = Sb, Bi, Ba), *Chem. Sci.*, 2022, **13**, 2640–2648.

[40] H. Lin, Y.-Y. Li, M.-Y. Li, Z. Ma, L.-M. Wu, X.-T. Wu and Q.-L. Zhu, Centric-to-acentric structure transformation induced by a stereochemically active lone pair: a new insight for design of IR nonlinear optical materials, *J. Mater. Chem. C*, 2019, **7**, 4638–4643.

[41] J. S. Knyrim, P. Becker, D. Johrendt and H. Huppertz, A New Non-Centrosymmetric Modification of BiB_3O_6, *Angew. Chem. Int. Ed.*, 2006, **45**, 8239–8241.

[42] Yan, H.-G. Xue and S.-P. Guo, Recent Achievements in Lone-Pair Cation-Based Infrared Second-Order Nonlinear Optical Materials, *Cryst. Growth Des.*, 2021, **21**, 698–720.

[43] Y. Chu, G. Li, X. Su, K. Wu and S. Pan, A review on the development of infrared nonlinear optical materials with triangular anionic groups, *J. Solid State Chem.*, 2019, **271**, 266–272.

[44] Y. Li, J. Luo and S. Zhao, Local Polarity-Induced Assembly of Second-Order Nonlinear Optical Materials, *Acc. Chem. Res.*, 2022, **55**, 3460–3469.

[45] *Bruker APEX4; Bruker AXS Inc.: Madison, WI, 2015*.

[46] G. M. Sheldrick, A short history of *SHELX*, *Acta Crystallogr A Found Crystallogr*, 2008, **64**, 112–122.

[47] J. Tauc, R. Grigorovici and A. Vancu, Optical Properties and Electronic Structure of Amorphous Germanium, *Phys. Stat. Sol. (b)*, 1966, **15**, 627–637.

[48] P. Makuła, M. Pacia and W. Macyk, How To Correctly Determine the Band Gap Energy of Modified Semiconductor Photocatalysts Based on UV–Vis Spectra, *J. Phys. Chem. Lett.*, 2018, **9**, 6814–6817.

[49] *O. Jepsen, A. Burkhardt and O. K Andersen, The Program TB-LMTO-ASA, Version4.7, Max-Planck-Institut Für Festkörperforschung, Stuttgart, Germany, 1999*.

[50] U. V. Barth and L. Hedin, A local exchange-correlation potential for the spin polarized case. i, *J. Phys. C: Solid State Phys.*, 1972, **5**, 1629–1642.

[51] S. K. Kurtz and T. T. Perry, A Powder Technique for the Evaluation of Nonlinear Optical Materials, *J. Appl. Phys.*, 1968, **39**, 3798–3813.

[52] D.-H. Kang and T. Schleid, $La_3S_2Cl_2[AsS_3]$: A Sulfide Chloride Thioarsenate(III) of Lanthanum, *Z. Kristallogr. Suppl.*, 2008, **28**, 46.

[53] D.-H. Kang, F. Ledderboge, H. Kleinke and T. Schleid, $Pr_3S_2Cl_2[AsS_3]$: A Praseodymium(III) Sulfide Chloride Thioarsenate(III) with Double Chains of Condensed $[SPr_4]^{10+}$ Tetrahedra: Praseodymium(III) Sulfide Chloride Thioarsenate(III), *Z. Anorg. Allg. Chem.*, 2015, **641**, 322–326.

[54] H.-J. Zhao, H.-D. Yang, P.-F. Liu and H. Lin, From *Cc* to $P6_3mc$: Structural Variation in $La_3S_2Cl_2[SbS_3]$ and $La_3OSCl_2[SbS_3]$ Induced by the Isovalent Anion Substitution, *Cryst. Growth Des.*, 2022, **22**, 1437–1444.

[55] H.-J. Zhao, P.-F. Liu and L.-M. Wu, Structural diversities in centrosymmetric $La_8S_4Cl_8$ $La_{12}S_8Cl_4[SbS_3]_8$ and non-centrosymmetric $Ln_{12}S_8Cl_8[SbS_3]_4$ (Ln = La and Ce): syntheses, crystal and electronic structures, and optical properties, *Dalton Trans.*, 2021, **50**, 2075–2082.

[56] G. Akopov, G. Viswanathan, N. W. Hewage, P. Yox, K. Wu and K. Kovnir, Pd and octahedra do not get along: Square planar [PdS4] units in non-centrosymmetric $La_6PdSi_2S_{14}$, *J. Alloys. Compd.*, 2022, **902**, 163756.

[57] Y. Yang, Y. Chu, B. Zhang, K. Wu and S. Pan, Unique Unilateral-Chelated Mode-Induced d–p–π Interaction Enhances Second-Harmonic Generation Response in New Ln_3LiMS_7 Family, *Chem. Mater.*, 2021, **33**, 4225–4230.

[58] P. Bonazzi, S. Menchetti and G. Pratesi, The crystal structure of pararealgar, As_4S_4, *Am Min*, 1995, **80**, 400–403.

[59] K. Iyer, J. B. Cho, M. J. Waters, J. S. Cho, B. M. Oxley, J. M. Rondinelli, J. I. Jang and M. G. Kanatzidis, Ba_2MAsQ_5 (Q = S and Se) Family of Polar Structures with Large Second Harmonic Generation and Phase Matchability, *Chem. Mater.*, 2022, **34**, 5283–5293.

[60] Y. Li, X. Cao, M. Ji, Z. You and Y. An, Solvothermal syntheses, structures, and characterizations of four thioarsenates $A_7Cu_4As_3S_{13}$ (A = Rb, Cs), $Rb_2Cu_5As_3S_8$, and CsCu2AsS3, *Inorg. Chem. Commun.*, 2022, **139**, 109365.

[61] D. Yan, Y. Xiao, C. Liu, P. Hou, W. Chai, H. Hosono, H. Lin and Y. Liu, Two new members in the quaternary Cs–Ag–As–S family with different arrangements of Ag–S and As–S asymmetric building units: syntheses, structures, and theoretical studies, *Dalton Trans.*, 2020, **49**, 9743–9750.

[62] J. E. Jerome, P. T. Wood, W. T. Pennington and J. W. Kolis, Synthesis of New Low-Dimensional Quaternary Compounds, KCu_2AsS_3 and KCu_4AsS_4, in Supercritical Amine Solvent. Alkali Metal Derivatives of Sulfosalts, *Inorg. Chem.*, 1994, **33**, 1733–1734.